J|A|C|S
ARTICLES

O-Atom Transport Catalysis by Atomic Cations in the Gas Phase: Reduction of N_2O by CO

Voislav Blagojevic, Galina Orlova, and Diethard K. Bohme*

*Contribution from the Department of Chemistry, Centre for Research in Mass Spectrometry and
Centre for Research in Earth and Space Science, York University, Toronto,
Ontario, Canada, M3J 1P3*

Received August 20, 2004; E-mail: dkbohme@yorku.ca

Abstract: Atomic cations (26), M^+, have been shown to lie within a thermodynamic window for O-atom transport catalysis of the reduction of N_2O by CO and have been checked for catalytic activity at room temperature with kinetic measurements using an inductively-coupled plasma/selected-ion flow tube (ICP/SIFT) tandem mass spectrometer. Only 10 of these 26 atomic cations were seen to be catalytic: Ca^+, Fe^+, Ge^+, Sr^+, Ba^+, Os^+, Ir^+, Pt^+, Eu^+, and Yb^+. The remaining 16 cations that lie in the thermodynamic window (Cr^+, Mn^+, Co^+, Ni^+, Cu^+, Se^+, Mo^+, Ru^+, Rh^+, Sn^+, Te^+, Re^+, Pb^+, Bi^+, Tm^+, and Lu^+) react too slowly at room temperature either in the formation of MO^+ or in its reduction by CO. Many of these reactions are known to be spin forbidden and a few actually may lie outside the thermodynamic window. A new measure of efficiency is introduced for catalytic cycles that allows the discrimination between catalytic cations on the basis of the efficiencies of the two legs of the catalytic cycle. Also, a potential-energy landscape is computed for the reduction of N_2O by CO catalyzed by $Fe^+(^6D)$ that vividly illustrates the operation of an ionic catalyst.

1. Introduction

The natural affinity of an atomic cation for an O atom can afford an alternate path for the transfer of an O atom from one molecule to another: the atomic cation simply picks up the O atom from a donor molecule and delivers it to an acceptor molecule (and in the process is regenerated). Furthermore, the extra dimension of charge brought to bear in this chemical transformation leads to a significant increase in the rate of both the O-atom pickup and the O-atom delivery: the overall O-atom transfer is catalyzed as well. The increase in these rates is a consequence of the electrostatic attraction between ions and molecules that acts to reduce kinetic activation energies. The first example of this “O-atom transport catalysis” of which we are aware, although not recognized as such at the time, is the reaction couple (eq 1) and (eq 2) reported in 1968 in the context of the chemistry of the earth’s ionosphere (the E-region):[1a]

$$Mg^+ + O_3 \rightarrow MgO^+ + O_2 \qquad (1)$$

$$MgO^+ + O \rightarrow Mg^+ + O_2 \qquad (2)$$

Both of these reactions are fast at 300 K, $k_1 = 2.3 \times 10^{-10}$ and $k_2 = 1 \times 10^{-10}$ cm^3 molecule^{-1} s^{-1}, as measured with the early flowing afterglow technique.[1a] Overall, the Mg^+ cations act to catalyze the reduction of ozone by atomic oxygen, reation 3, which proceeds with a rate coefficient $k = 9.1 \times 10^{-15}$ cm^3 molecule^{-1} s^{-1} at room temperature ($E_a = 4.4$ kcal mol^{-1}).[1b]

$$O_3 + O \rightarrow O_2 + O_2 \qquad (3)$$

Of atmospheric interest at the time was that reaction 2 keeps Mg^+/MgO^+ large in the E region (where MgO^+ can be lost by recombination with electrons) and not that reactions 1 and 2 constitute a catalytic cycle for the reduction of O_3 by O.

The landmark experiments of Kappes and Staley in 1981 demonstrated the first cyclic reduction of N_2O by CO in the gas phase in the presence of atomic metal cations.[2] These authors reported the occurrence, in an ion-cyclotron resonance (ICR) spectrometer, of reactions 4 and 5 in which the Fe^+ cation acts as a catalyst for the overall transformation given by reaction 6.

$$Fe^+ + N_2O \rightarrow FeO^+ + N_2 \qquad (4)$$

$$FeO^+ + CO \rightarrow Fe^+ + CO_2 \qquad (5)$$

$$N_2O + CO \rightarrow N_2 + CO_2 \qquad (6)$$

The reported rate coefficients were $k_4 = 7 \times 10^{-11}$ and $k_5 = 9 \times 10^{-10}$ cm^3 molecule^{-1} s^{-1}. Five other transition-metal cations, Ti^+, Zr^+, V^+, Nb^+, and Cr^+, were tried but were found not to act as catalysts in that the oxides of these metal cations were observed not to be reduced by CO with a measurable rate. Selected-ion flow tube (SIFT) experiments in 1995 provided somewhat lower rate coefficients for $k_4 = 3.1 \times 10^{-11}$ and k_5

---

(1) (a) Ferguson, E. E.; Fehsenfeld, F. C. *J. Geophys. Res.* **1968**, *73*, 6215−6223. (b) Kaufman, F. Defense Nuclear Agency Reaction Rate Handbook, 2nd ed.; DASIAC, General Electric, TEMPO: Santa Barbara, California, 1972; Chapter 19.

(2) Kappes, M. M.; Staley, R. H. *J. Am. Chem. Soc.* **1981**, *103*, 1286.

10.1021/ja044950m CCC: $30.25 © 2005 American Chemical Society

Scheme 1

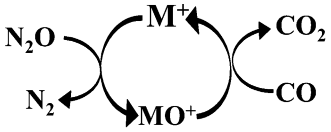

$= 2.05 \times 10^{-10}$ cm^3 molecule^{-1} s^{-1} at room temperature and also demonstrated that the catalytic cycle is not poisoned by N_2O, since $FeO(N_2O)_n^+$ remains reactive at least up to $n = 3$ according to reaction 7.[3]

$$FeO(N_2O)_n^+ + CO \rightarrow Fe^+ + (CO_2 + nN_2O) \qquad (7)$$

More recently Pt^+ has been shown to undergo reactions of type 4 and 5 with $k = 7 \times 10^{-11}$ and $k = 6.7 \times 10^{-10}$ cm^3 molecule^{-1} s^{-1}, respectively, which means that Pt^+ can catalyze reaction 6 as well.[4] In our laboratory, using ICP-SIFT tandem mass spectrometry, we have recently confirmed the catalytic activity of Fe^+, were able to add Os^+ and Ir^+ to the list of catalysts active in the reduction of N_2O by CO, and extended observations of atomic metal-cation catalysis to the reduction of NO_2 and NO by CO.[5a] Very recently platinum cluster cations, Pt_n^+ ($n =$ 6−8), also have been observed to catalyze reaction 6.[5b]

Here we ask whether the four atomic ions, Fe^+, Pt^+, Os^+, and Ir^+, represent a complete set of atomic cations effective as catalysts in the reduction of N_2O by CO and if not, why not? In answering these questions, we formulate a general thermodynamic requirement for this catalysis and extend the kinetic measurements to 22 other atomic cations that meet this requirement. The 22 atomic cations are chosen from the first-row atomic cations from K^+ to Se^+, the second-row atomic cations from Rb^+ to Te^+ (excluding Tc^+) and the third-row atomic cations from Cs^+ to Bi^+, as well as the lanthanide cations (excluding Pm^+).

Since the reduction of N_2O by CO involves the transfer of an O atom from N_2O to CO, an atomic metal cation M^+ must have an O-atom affinity that lies between OA(N_2) and OA(CO) to have the thermodynamic potential to catalyze reaction 6. Available O-atom affinities[6] indicate a thermodynamic "window" of 87 kcal mol^{-1}, 40 kcal mol^{-1} < OA(M^+) < 127 kcal mol^{-1}, and that 26 of the 59 first, second, third row and lanthanide cations that we have investigated meet, within the uncertainties of the known O-atom affinities, the thermodynamic criterion for the catalytic reduction of N_2O by CO according to reactions 8 and 9 and illustrated in Scheme 1.

$$M^+ + N_2O \rightarrow MO^+ + N_2 \qquad (8)$$

$$MO^+ + CO \rightarrow M^+ + CO_2 \qquad (9)$$

However, we will show that less than half of these 26 cations have the required kinetic properties to exhibit this catalysis to a measurable extent. Furthermore, the versatility of the ICP-SIFT tandem mass spectrometer used in these experiments has provided a means to track the steady-state achieved in these catalytic cycles. Also, we were able to explore the action of higher oxide cations as catalysts and the influence of N_2O ligation on the catalytic activity of atomic ions.

2. Methods Section

2.1. Experimental Methods. The reactions were investigated in an inductively-coupled plasma/selected-ion flow tube (ICP/SIFT) tandem mass spectrometer. The apparatus has been described previously.[7] Elemental cations of interest are generated in an argon plasma operating at atmospheric pressure and ca. 5500 K fed with a dilute solution of salts containing the corresponding element. The ions are introduced into a differentially pumped sampling interface, then mass selected by a quadrupole mass filter, and injected into a flow tube flushed with He buffer gas at 0.35 Torr and 295 ± 2 K. The metal ions cool by radiation and collision with argon and helium from their point of origin in the ICP to the entrance of the reaction region. The state distribution of the ICP ions and their relaxation by collision and radiation before they reach the reaction region have been discussed in detail previously.[8] Neutral reagent molecules were added downstream into the reaction region. Ions present in the reacting mixtures were sampled by a second quadrupole mass spectrometer.

In our previous studies of reactions of atomic metal cations with N_2O,[8] the N_2O was added directly into the reaction region downstream in the flow tube. Rate coefficients for the oxidation reactions of M^+ were derived from the linear semilogarithmic decays of M^+ in the usual way using pseudo first-order kinetics.[7−9] In the studies reported here of atomic-oxide cation chemistry with CO, the atomic-oxide cation was produced upstream from the reaction of the atomic ion with N_2O, and CO was introduced into the reaction region further downstream. Due to the presence of N_2O in the reaction region, a steady state was established between the oxidation reaction of M^+ with N_2O and the reduction reaction of MO^+ with CO. Only *lower limits* to the rate coefficients could be obtained for the reduction reactions from the initial tangent to the curved semilogarithmic decays of MO^+. To obtain absolute values for the rate coefficients of the reduction reactions we took advantage of the establishment of a steady state and used the steady-state analysis described in the text to derive the rate coefficient for the reduction reaction.

All measurements were performed at room temperature of 295 ± 2 K and at a helium operating pressure of 0.35 ± 0.01 Torr. The nitrous oxide was obtained commercially and was of high purity (Matheson Gas products, >98.0%). The carbon monoxide was of C. P. Grade (99.5%) and obtained from Canadian Liquid Air Ltd.

2.2. Computational Methods. We have performed a density functional theory (DFT) study of the reactions $N_2O + CO \rightarrow CO_2 + N_2$ (closed singlet) and $Fe^+ + N_2O \rightarrow MO^+ + N_2$ and $FeO^+ + CO \rightarrow Fe^+ + CO_2$ (sextet electronic state). All theoretical predictions were made using the Gaussian98 program suite[10] with the hybrid B3LYP[11,12]

---

(3) Baranov, V.; Javahery, G.; Hopkinson, A. C.; Bohme, D. K. *J. Am. Chem. Soc.* **1995**, *117*, 12801.

(4) Brönstrup, M.; Schröder, D.; Kretzschmar, I.; Schwarz, H.; Harvey, J. N. *J. Am. Chem. Soc.* **2001**, *123*, 142.

(5) (a) Blagojevic, V.; Jarvis, M. J. Y.; Flaim, E.; Koyanagi, G. K.; Lavrov, V. V.; Bohme, D. K. *Angew. Chem.* **2003**, *115*, 5053; *Angew. Chem., Int. Ed.* **2003**, *42*, 4923. (b) Balaj, O. P.; Balteanu, I.; Rossteuscher, T. T. J.; Beyer, M. K.; Bondybey, V. E. *Angew. Chem.* **2004**, *116*, 6681; *Angew. Chem. Int. Ed.* **2004**, *47*, 6519.

(6) Lias, S. G.; Bartmess, J. E.; Liebman, J. F.; Holmes, J. L.; Levin, R. D.; Mallard, W. G. *J. Phys. Chem. Ref. Data* **1988**, *17* (Suppl 1).

(7) Koyanagi, G. K.; Lavrov, V. V.; Baranov, V. I.; Bandura, D.; Tanner, S. D.; McLaren, J. W.; Bohme, D. K. *Int. J. Mass Spectrom.* **2000**, *194*, L1.

(8) Lavrov, V. V.; Blagojevic, V.; Koyanagi, G. K.; Orlova, G.; Bohme, D. K. *J. Phys. Chem. A* **2004**, *108*, 5610.

(9) (a) Mackay, G. I.; Vlachos, G. D.; Bohme, D. K.; Schiff, H. I. *Int. J. Mass Spectrom. Ion Phys.* **1980**, *36*, 259. (b) Raksit, A. B.; Bohme, D. K. *Int. J. Mass Spectrom. Ion Processes* **1983**, *55*, 69.

(10) Frisch, M. J.; Trucks, G. W.; Schlegel, H. B.; Scuseria, G. E.; Robb, M. A.; Cheeseman, J. R.; Zakrzewski, V. G.; Montgomery, J. A., Jr.; Stratmann, R. E.; Burant, J. C.; Dapprich, S.; Millam, J. M.; Daniels, A. D.; Kudin, K. N.; Strain, M. C.; Farkas, O.; Tomasi, J.; Barone, V.; Cossi, M.; Cammi, R.; Mennucci, B.; Pomelli, C.; Adamo, C.; Clifford, S.; Ochterski, J.; Petersson, G. A.; Ayala, P. Y.; Cui, Q.; Morokuma, K.; Malick, D. K.; Rabuck, A. D.; Raghavachari, K.; Foresman, J. B.; Cioslowski, J.; Ortiz, J. V.; Stefanov, B. B.; Liu, G.; Liashenko, A.; Piskorz, P.; Komaromi, I.; Gomperts, R.; Martin, R. L.; Fox, D. J.; Keith, T.; Al-Laham, M. A.; Peng, C. Y.; Nanayakkara, A.; Gonzalez, C.; Challacombe, M.; Gill, P. M. W.; Johnson, B. G.; Chen, W.; Wong, M. W.; Andres, J. L.; Head-Gordon, M.; Replogle, E. S.; Pople, J. A. *Gaussian 98*, revision A.11; Gaussian, Inc.: Pittsburgh, PA, 1998.

Table 1. Rate Coefficients for Reactions of Atomic-metal Cations M^+ with N_2O and of Metal-Monoxide Cations MO^+ with CO Measured at Room Temperature Using an ICP/SIFT Tandem Mass Spectrometer[a]

		$M^+ + N_2O$		$MO^+ + CO$		
M^+	$OA(M^+)$[b]	k[c]	products	k[c]	products	k[d]
Ca^+	77.2	1.6×10^{-10}	CaO^+	$\geq 5.7 \times 10^{-12}$	Ca^+	2.5×10^{-10}
Cr^+	85.8 ± 2.8	1.5×10^{-13}	CrO^+ (0.98) $Cr^+ \cdot N_2O$ (0.02)	$<10^{-13}$		
Mn^+	68.0 ± 3.0	$<10^{-13}$	$Mn^+ \cdot N_2O$	NA		
Fe^+	80.0 ± 1.4	3.7×10^{-11}	FeO^+	$\geq 2.4 \times 10^{-10}$ [c]	Fe^+	1.8×10^{-10}
Co^+	74.9 ± 1.2	2.1×10^{-12}	CoO^+ (0.50) $Co^+ \cdot N_2O$ (0.50)	$<10^{-13}$		
Ni^+	63.2 ± 1.2	6.5×10^{-13}	$Ni^+ \cdot N_2O$	NA		
Cu^+	37.4 ± 3.5	5.7×10^{-13}	$Cu^+ \cdot N_2O$	NA		
Ge^+	81.8	3.6×10^{-10}	GeO^+	$\geq 1.1 \times 10^{-10}$	Ge^+	2.1×10^{-10}
Se^+	92	1.8×10^{-12}	SeO^+	NA		
Sr^+	71.4	6.3×10^{-11}	SrO^+	$\geq 8.7 \times 10^{-10}$	Sr^+	1.0×10^{-10}
Mo^+	116.7 ± 0.5	3.4×10^{-13}	$Mo^+ \cdot N_2O$	NA		
Ru^+	87.9 ± 1.2	3.3×10^{-13}	$Ru^+ \cdot N_2O$	NA		
Rh^+	69.6 ± 1.4	4.0×10^{-13}	$Rh^+ \cdot N_2O$	NA		
Sn^+	75.1	1.0×10^{-13}	$Sn^+ \cdot N_2O$	NA		
Te^+	96.6	$<10^{-13}$	none	NA		
Ba^+	92.8	2.4×10^{-10}	BaO^+	$\geq 3.1 \times 10^{-11}$	Ba^+	2.3×10^{-11}
Re^+	115 ± 15	$<10^{-13}$	ReO^+	NA		
Os^+	100 ± 12	5.8×10^{-10}	OsO^+ (0.40) OsN^+ (0.60)	$\geq 4.6 \times 10^{-11}$	Os^+	$\geq 4.0 \times 10^{-13}$ [e]
Ir^+	59	2.9×10^{-10}	IrO^+	$\geq 2.6 \times 10^{-11}$	Ir^+	3.5×10^{-10}
Pt^+	77	1.2×10^{-10}	PtO^+	$\geq 1.2 \times 10^{-10}$	Pt^+	2.3×10^{-10}
Pb^+	53.2	$<10^{-13}$	$Pb^+ \cdot N_2O$	NA		
Bi^+	41.6	$<10^{-13}$	$Bi^+ \cdot N_2O$	NA		
Eu^+	93.2 ± 4.3	6.9×10^{-11}	EuO^+	$\geq 3.3 \times 10^{-12}$	Eu^+	NA
Tm^+	116.6 ± 4.3	4.4×10^{-12}	TmO^+	$<10^{-13}$		
Yb^+	88.1 ± 5.9	6.5×10^{-13}	YbO^+	$\geq 1.2 \times 10^{-11}$	Yb^+	1.2×10^{-11}
Lu^+	128.0 ± 4.3	2.6×10^{-10}	LuO^+	$<10^{-13}$		

[a] All the metal cations shown are known to have $OA(N_2) < OA(M^+) < OA(CO)$ within the uncertainties of the known O-atom affinities. [b] OA is the oxygen-atom affinity in kcal mol^{-1} (see ref 8 for leading references). [c] k is the reaction rate coefficient measured in units of cm^3 $molecule^{-1}$ s^{-1} with an uncertainty less than ±30%. NA (not available) indicates that the rate coefficient could not be measured because MO^+ could not be established in sufficient amounts. [d] Rate coefficients in units of cm^3 $molecule^{-1}$ s^{-1} obtained from steady-state analysis (see text). Unless indicated otherwise, the estimated uncertainty is ±40%. [e] This value is a lower limit because of overlap of OsO^+ with unreactive OsN^+.

exchange-correlation functional. The triply split 6-311+G(d) basis set[13,14] with one set of diffuse and polarization functions[15,16] was used for all atoms. Harmonic vibrational frequencies were computed to verify minima (all real frequencies) and transition state structures (one imaginary frequency). The connections between transition states and corresponding minima were verified using an intrinsic reaction coordinate technique (IRC) developed by Gonzalez and Schlegel.[17,18] Relative enthalpies at 0 K are reported. Cartesian coordinates and electronic energies for all optimized structures are available as Supporting Information.

3. Results and Discussion

3.1. Thermodynamic Window for O-Atom Transport. The O-atom affinity of nitrogen to form nitrous oxide, $OA(N_2)$, is 39.95 ± 0.02 kcal mol^{-1} and that for CO to form CO_2, OA(CO), is 127.3 ± 0.02 kcal mol^{-1}.[6] This means that the “thermodynamic window of opportunity” for O-atom transport catalysis of reaction 6 is given by 40 kcal $mol^{-1} < OA(M^+) <$ 127 kcal mol^{-1}.

Of the 59 atomic cations now routinely investigated in our laboratory, 26 fall within this thermodynamic window within the uncertainties of their known O-atom affinities. The known O-atom affinities of these 26 cations are included in Table 1. Two of them, $OA(Cu^+)$ and $OA(Lu^+)$, are borderline.

3.2. Summary of the Kinetics of Metal-Cation Oxidation Reactions with N_2O. Reactions of M^+ with N_2O, reaction 8, constitute the first leg of the catalytic cycle shown in Scheme 1 and can be measured with the ICP/SIFT tandem mass spectrometer simply by adding N_2O into the reaction region of the flow tube. This has been done very recently and reported by us for first, second, and third row atomic cations,[8] as well as for lanthanide cations.[19] We found that O-atom transfer was a predominant, although not exclusive, reaction channel. Both N-atom transfer and N_2O addition were observed to compete with O-atom transfer according to reaction 10.

$$M^+ + N_2O \rightarrow MO^+ + N_2 \qquad (10a)$$

$$\rightarrow MN^+ + NO \qquad (10b)$$

$$\rightarrow M^+N_2O \qquad (10c)$$

The measured rate coefficients and product distributions that

---

(11) Becke, A. D. *J. Chem. Phys.* **1993**, *98*, 5648.
(12) Lee, C.; Yang, W.; Parr, R. G. *Phys. Rev. B* **1988**, *37*, 785.
(13) Hehre, W. J.; Ditchfield, R.; Pople, J. A. *J. Chem. Phys.* **1972**, *56*, 2257.
(14) Krishnan, R.; Binkley, J. S.; Seeger, R.; Pople, J. A. *J. Chem. Phys.* **1980**, *72*, 650.
(15) Chandrasekhar, J.; Andrade, J. G.; Schleyer, P. v. R. *J. Am. Chem. Soc.* **1981**, *103*, 5609.
(16) Clark, T.; Chandrasekhar, J.; Spitznagel, G. W.; Schleyer, P.v. R. *J. Comput. Chem.* **1983**, *4*, 294.
(17) Gonzalez, C.; Schlegel, H. B. *J. Chem. Phys.* **1989**, *90*, 3154.
(18) Gonzalez, C.; Schlegel, H. B. *J. Phys. Chem.* **1990**, *94*, 5523.
(19) Rowe, B. R.; Viggiano, A. A.; Fehsenfeld, F. C.; Fahey, D. W.; Ferguson, E. E. *J. Chem. Phys.* **1982**, *75*, 742.

we have measured previously[8,19] for the 26 cations within the thermodynamic window for O-atom transport catalysis are given in Table 1. Os^+ is the only cation in this list that exhibits N-atom transfer along with O-atom transfer while Cr^+ and Co^+ show some N_2O addition. The rates of O-atom transfer exhibit interesting variations: the measured rate coefficients for the 26 cations in question range from $<10^{-13}$ to 5.8×10^{-10} cm^3 molecule^{-1} s^{-1}. We have discussed previously that kinetic constraints for these exothermic reactions arise in a number of ways. There may be a genuine activation barrier in the reaction coordinate, as is the case for the reactions with Fe^+ and Rh^+ according to our computations.[8] The reaction may be spin forbidden overall, as is the case with Cr^+, Mn^+, Co^+, Ni^+, Mo^+, Ru^+.[8] In the case of the lanthanide cations (Eu^+, Tm^+, Yb^+, Lu^+), a barrier to reaction may arise from the energy associated with the promotion of a 4f electron to make two electrons available for bonding.[19] The reaction may be endothermic within the uncertainty of the known oxygen-atom affinity (Cu^+) or the lowest spin-allowed channel may be endothermic (Co^+). For the remaining atomic ions that react slowly (as is the case with Se^+, Sn^+, Te^+, Re^+, Pb^+, Bi^+) there is insufficient information available about the energy profile for reaction to provide an explanation for their low O-atom transfer reactivity. Ten atomic ions (Mn^+, Ni^+, Cu^+, Mo^+, Ru^+, Rh^+, Sn^+, Pb^+, Bi^+) simply added N_2O and Te^+ did not show any products at all under our experimental operating conditions.

Of the 26 cations that lie within the thermodynamic window for O-atom transport catalysis, only 14 (Ca^+, Cr^+, Fe^+, Co^+, Ge^+, Sr^+, Ba^+, Os^+, Ir^+, Pt^+, Eu^+, Tm^+, Yb^+, and Lu^+) react sufficiently quickly with N_2O to establish large enough concentrations of MO^+ to obtain meaningful results for its reaction under our experimental conditions. Two cations (Se^+, Re^+) produce insufficient amounts of the oxide cation.

Higher-order addition reactions with N_2O were observed with some of the oxide cations at the flows of N_2O that were employed. The $MO^+(N_2O)$ adduct was observed for M = Ca, Fe, Sr, Ba, Eu and Lu. Only the $EuO^+(N_2O)$ adduct ion appeared to react with CO by exchanging the N_2O for CO. Also observed were $PtO_2^+(N_2O)$ and $BaO^+(N_2O)_2$. The oxide cations OsO^+, IrO^+, and PtO^+ reacted further with N_2O by sequential O-atom transfer to form the higher oxides OsO_n^+ ($n = 2, 3, 4$), IrO_n^+ ($n = 2, 3$), and PtO_n^+ ($n = 2, 3$), respectively. We can also report here a rate coefficient of 5.8×10^{-10} cm^3 molecule^{-1} s^{-1} for the oxidation of PtO^+ with N_2O to form PtO_2^+.

3.3. Reduction Reactions of Metal-Monoxide Cations with CO. Of the 16 oxide cations that could be produced by the reactions of M^+ cations that reacted with N_2O, only 10 exhibited an observable reaction with CO: CaO^+, FeO^+, GeO^+, SrO^+, BaO^+, OsO^+, IrO^+, PtO^+, EuO^+, and YbO^+. Four other atomic oxide cations (CrO^+, CoO^+, TmO^+, and LuO^+) were observed not to react with CO, $k < 10^{-13}$ cm^3 molecule^{-1} s^{-1}, and two (SeO^+, ReO^+) were simply too small in intensity to provide any kind of measurement.

Experimental results obtained for the 10 oxide cations that were observably reactive with CO at a fixed N_2O flow are shown in Figures 1 to 3. The solid lines represent kinetic fits to the data points. The fitting of the ion profiles was performed in several different ways depending on the nature of the ion. Where possible, the decays of reactant ions were fitted using kinetic equations for pseudo-first-order reactions. When this was not possible due to the occurrence of reaction 8 in the reaction region we used two and three component fits originally developed for multicomponent reactions. Although this latter approach provides a fit to the data, it is quite arbitrary, usually has no real physical meaning and was not used to extract rate coefficients. However, in those cases where the observed curvature actually is due to the presence of two isomers, e.g., IrO_3^+ and $CaO^+(N_2O,CO_2)_2$, the fits do have physical meaning. Where possible, the N_2O flow was adjusted to establish the MO^+ ion as the predominant ion before CO addition. This was not achieved with YbO^+ because of the slow reaction of Yb^+ with N_2O and with OsO^+, IrO^+, and PtO^+ because of their fast reactions with N_2O to form higher oxide cations. With EuO^+ the N_2O flow needed to be reduced to maximize the decay of EuO^+ because of its relatively slow reduction with CO (reaction 8 is much faster than reaction 9). The limits to the rate coefficients for the reduction reactions that could be determined from the initial slopes of the curved decays observed for MO^+ are included in Table 1.

3.3.1. Alkaline-Earth Oxide Cations: CaO^+, SrO^+, BaO^+. The reductions of CaO^+, SrO^+, and BaO^+ with CO according to reaction 9 are clearly evident in Figure 1. In the special case of CaO^+, overlap in the ion signal was observed with $C_2O_2^+$ produced by the reaction of CO with CO^+ produced by chemistry initiated by Ar^+ that could not be separated from Ca^+ with the upstream quadrupole. The N_2O adducts of CaO^+, SrO^+, and BaO^+ formed upstream of the reaction region at the flows of N_2O used in these experiments all showed reactivity with CO. Two product channels come into question, and these are shown in reaction 11.

$$MO^+(N_2O) + CO \rightarrow MO^+ + (N_2 + CO_2) \qquad (11a)$$

$$\rightarrow M^+ + (N_2O + CO_2) \qquad (11b)$$

Channel 11a can be viewed as a neutral reaction between N_2O and CO driven by the bond activation of N_2O by CaO^+. Such bond-activation reactions have been reported previously.[19,20]

A more exothermic variant of reaction 11a is reaction 12 in which CO_2 remains attached to MO^+. Here the ionic product is isobaric with the ionic reactant.

$$MO^+(N_2O) + CO \rightarrow MO^+(CO_2) + N_2 \qquad (12)$$

Channel 11b corresponds to an O-atom transfer in which N_2O is liberated. Both channels are exothermic. Channel 11a is exothermic by the exothermicity of the neutral reaction, $N_2O + CO \rightarrow N_2 + CO_2$, less $D(MO^+ - N_2O)$, viz. $\Delta H(11a) = -80$ kcal mol^{-1} + $D(MO^+ - N_2O)$. For channel 11b, $\Delta H(11b) = OA(M^+) - OA(CO) + D(MO^+ - N_2O)$. Since $OA(M^+) - OA(CO) = -50, -56$, and -34 kcal mol^{-1} for $M^+ = Ca^+, Sr^+$, and Ba^+, respectively, channel 11a is more exothermic than channel 11b. Our experiments indicate that channels 11a and 12 occur for M = Ca: a definite rise in the CaO^+ signal was associated with the disappearance of $CaO^+(N_2O)$, and a flattening in the $m/z = 100$ signal which we attribute to

---

(20) Viggiano, A. A.; Deakyne, C. A.; Dale, F.; Paulson, J. F. *J. Chem. Phys.* **1987**, *87*, 6544.

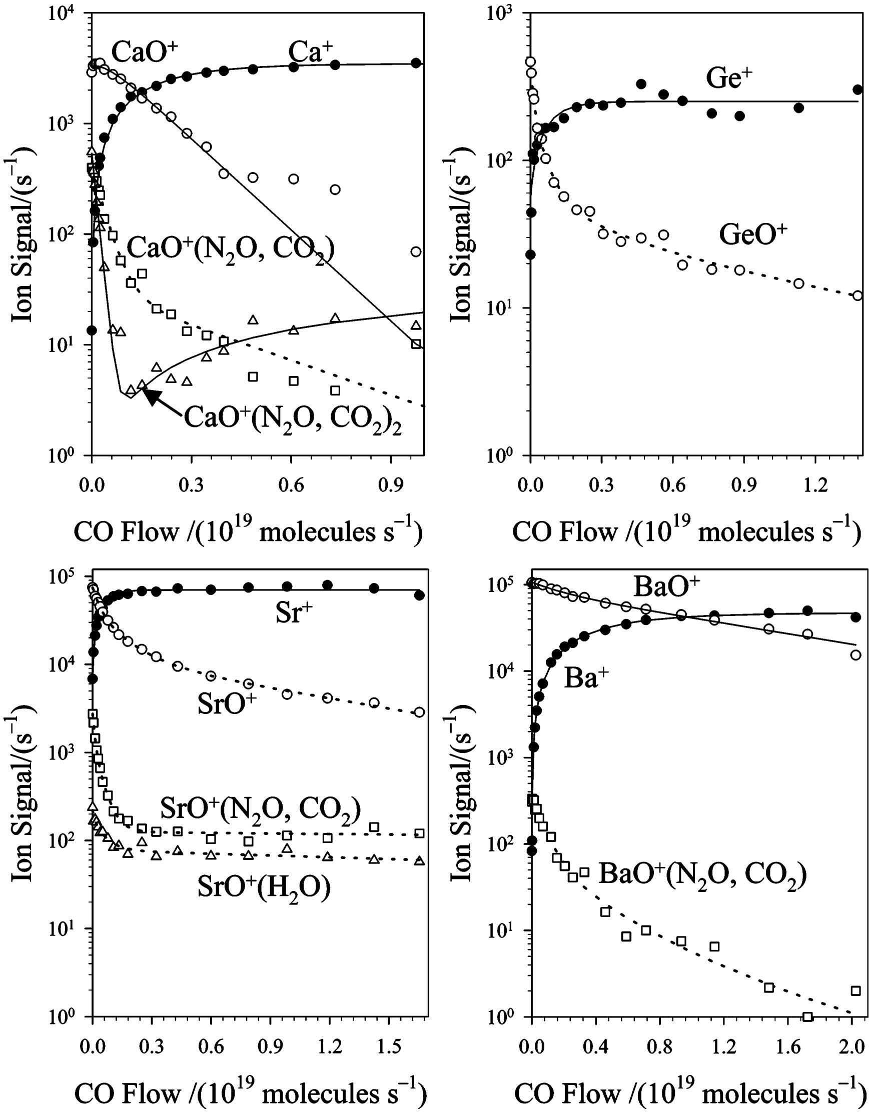

Figure 1. Ion profiles recorded for the chemistry initiated by CaO^+, GeO^+, SrO^+, and BaO^+ with carbon monoxide at 295 K in helium buffer gas at 0.35 Torr. The CaO^+ profile has been corrected for overlap with $C_2O_2^+$ (see text). The flows of N_2O added upstream are 0.8, 0.2, 2, and 1 × 10^{18} molecules s^{-1}. Dashed lines are nonkinetic fits. Solid lines are kinetic fits based on the initial slopes of the decays of relevant precursor ions.

$CaO^+(CO_2)$ is seen at high flows of CO (see Figure 1). The analogues of reactions 11a and 12 involving the second N_2O adduct of CaO^+, viz. reactions 13 and 14,

$$CaO^+(N_2O)_2 + CO \rightarrow CaO^+ + (N_2O + CO_2 + N_2) \quad (13)$$

$$CaO^+(N_2O)_2 + CO \rightarrow CaO^+(N_2O)(CO_2) + N_2 \quad (14)$$

also appear to occur; this time an ion with the mass of $CaO^+(N_2O)(CO_2)$ that can be produced by reaction 14 shows a definite increase at higher CO flows (see Figure 1). Reactions 11a and 12 also appear to occur for M = Sr: we attribute the flattening in the $m/z = 148$ signal to the formation of $SrO^+(CO_2)$ at high flows of CO. Also, it appears that this ion can exchange ligands according to reaction 15

$$SrO^+(CO_2) + H_2O \rightarrow SrO^+(H_2O) + CO_2 \quad (15)$$

with the water impurity in the buffer gas. In comparison, reaction 12 appears to contribute little, if at all, to a formation of $m/z = 198$ ($BaO^+(CO_2)$) at high flows of CO. We attribute the loss of the ion at $m/z = 198$ to the analogue of reaction 11a, but we cannot exclude the occurrence of the analogue of reaction 12.

3.3.2. GeO^+. The measurements for the reaction of GeO^+ with CO were simplified by the absence of N_2O adduct ions. As shown in Figure 1, only Ge^+ was observed as a product ion that was formed by reaction 9 (M = Ge) with $k \geq 1.1 \times 10^{-10}$ cm^3 $molecule^{-1}$ s^{-1}.

3.3.3. FeO^+. Figure 2 shows ion profiles for the reaction of FeO^+ with CO, reaction 5. Experiments at low flows of N_2O indicate a lower limit of $k \geq 2.4 \times 10^{-10}$ cm^3 $molecule^{-1}$ s^{-1} for this reaction. This value is in agreement with our earlier SIFT value of $k = 2.05(\pm 30\%) \times 10^{-10}$ cm^3 $molecule^{-1}$ s^{-1} determined from experiments in which FeO^+ was produced from a 1% mixture of $Fe(CO)_5$ in N_2O in an electron-impact ion source.[3]

FeO^+ readily adds N_2O in a sequential fashion,[3] and this accounts for the initial presence of $FeO^+(N_2O)_{1,2,3}$ in the reaction profiles shown in Figure 2. Careful inspection of the profiles of $FeO^+(N_2O)_{1,2,3}$ at very low flows of CO clearly indicates

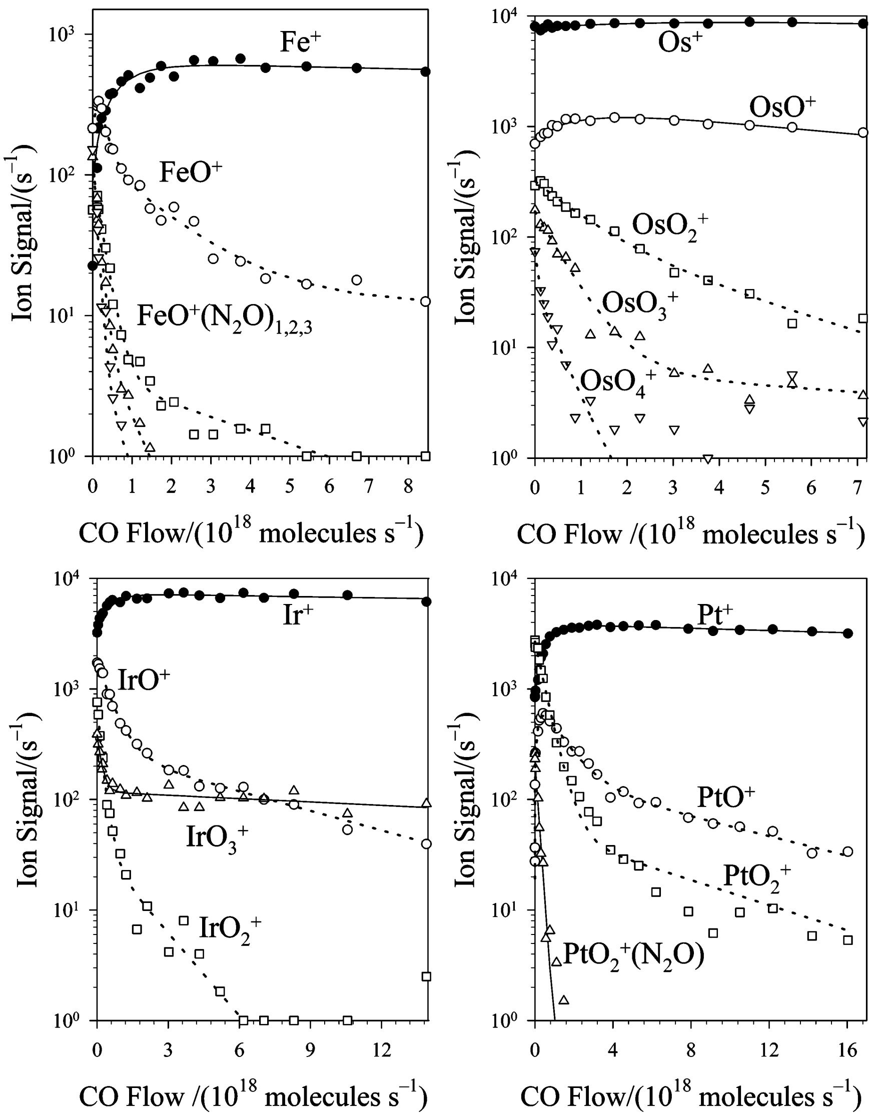

Figure 2. Ion profiles recorded for the chemistry initiated by FeO^+, OsO^+, IrO^+, and PtO^+ with carbon monoxide at 295 K in helium buffer gas at 0.35 Torr. The flows of N_2O added upstream are 2.5, 0.03, 0.2, and 0.4 × 10^{18} molecules s^{-1}. Dashed lines are nonkinetic fits. Solid lines are kinetic fits based on the initial slopes of the decays of relevant precursor ions.

the production of FeO^+ and $FeO^+(N_2O)$, and by analogy $FeO^+(N_2O)_2$, by reaction 16.

$$FeO^+(N_2O)_{1,2,3} + CO \rightarrow FeO^+(N_2O)_{0,1,2} + (N_2 + CO_2) \tag{16}$$

The disappearance of these ions had previously been attributed to reaction 17.

$$FeO(N_2O)_n{}^+ + CO \rightarrow Fe^+ + (CO_2 + nN_2O) \tag{17}$$

The conditions of the latter experiments were not varied sufficiently to discern the production of $FeO^+(N_2O)_{0,1,2}$ by reaction 16.

3.3.4. OsO^+, IrO^+, PtO^+. The profiles shown in Figure 2 for the reactions of the oxide cations of the platinum-group elements Os, Ir, and Pt all show similar chemistry. The initial slopes for the semilogarithmic decays of the oxide cations indicate limits of $\geq 4.6 \times 10^{-11}$, $\geq 2.6 \times 10^{-11}$, and $\geq 1.2 \times 10^{-10}$ cm^3 molecule^{-1} s^{-1} for the rate coefficients for reaction 9 with M = Os, Ir, and Pt, respectively. Analysis of the OsO^+ profile was complicated because of OsN^+ production (60%) in the reaction of Os^+ with N_2O[5,8] and some overlap between OsN^+ and OsO^+. However, OsN^+ appeared to be unreactive with CO so that the overlap could be corrected for.

Higher-order N_2O chemistry with OsO^+, IrO^+, and PtO^+ leads to formation of higher oxide cations according to reaction 18 with M = Os ($x = 1-4$), Ir ($x = 1-3$), and Pt ($x = 1-3$).[5,8]

$$MO_x{}^+ + CO \rightarrow MO_{x-1}{}^+ + CO_2 \tag{18}$$

The results with Os again were more complicated, in this case by the partial overlap of $OsO_x{}^+$ with $OsNO_{x-1}{}^+$ formed by the sequential oxidation of OsN^+ by N_2O.[8] The $OsNO_{x-1}{}^+$ ions appeared to be reduced by CO according to reaction 19.

$$OsNO_{x-1}{}^+ + CO \rightarrow OsNO_{x-2}{}^+ + CO_2 \qquad x = 2-4 \tag{19}$$

The ion with m/z corresponding to $IrO_3{}^+$ showed unusual behavior in that about 10% of this ion appeared not to react. It is possible that $IrO_3{}^+$ formed by the reaction of $IrO_2{}^+$ with N_2O is produced in two isomeric forms, one involving three $Ir^+{-}O$

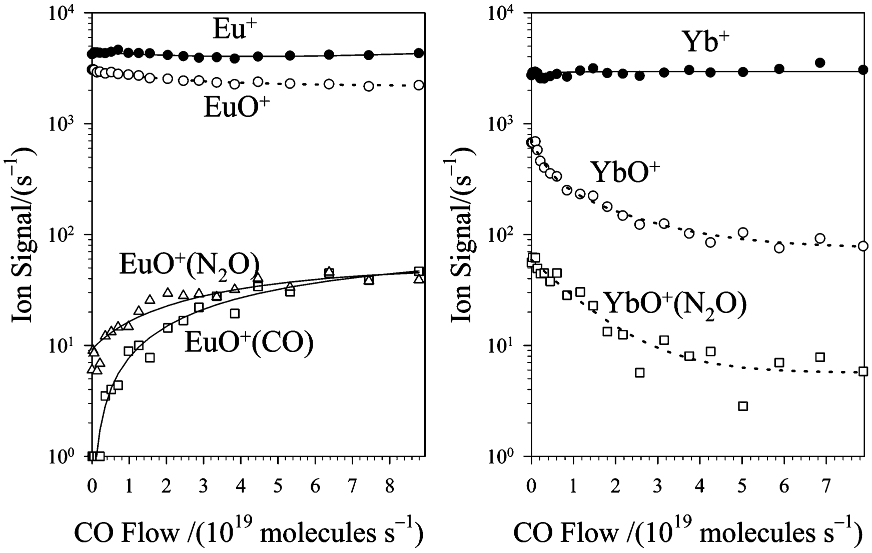

Figure 3. Ion profiles recorded for the chemistry initiated by EuO^+ and YbO^+ with carbon monoxide at 295 K in helium buffer gas at 0.35 Torr. The flows of N_2O added upstream are 3 and 4×10^{17} molecules s^{-1}. The initial slopes in the decays of MO^+ were used to fit the formation of product ions (solid lines).

bonds and the second one with an O—O bond and superoxide-like structure ($O{=}Ir^+{-}O{-}O$). Due to the difference in binding, one of the isomers would be quickly reduced by CO, while the reduction of the other isomer would proceed much slower, possibly due to presence of an activation barrier. However, in principle, we cannot rule out the initial formation of some hot or electronically excited ions of one structure from the reaction of IrO_2^+ with N_2O. The rapid disappearance with CO addition of the observed adduct ion $PtO_2^+(N_2O)$ is attributed to reaction 20 which is analogous to reaction 16.

$$PtO_2^+(N_2O) + CO \rightarrow PtO_2^+ + (N_2 + CO_2) \qquad (20)$$

3.3.5. Lanthanum Oxide Cations: EuO^+, YbO^+. The lanthanide cations Eu^+ and Yb^+ are borderline catalysts from the kinetic point of view (see Figure 3): they abstract an O atom from N_2O only very slowly, particularly Yb^+, because of the relatively large energy required to promote one electron from the $4f^n5d^06s^1$ to the $4f^{n-1}5d^16s^1$ configuration and so to make two electrons available for bonding with O.[21] The reduction of the oxide cations with CO also appears slow, although only lower limits to the rate coefficients could be obtained (see Table 1). The reduction of EuO^+ competes with addition of CO (<20% at the He pressure of our experiments), as some formation of $EuO^+(CO)$ was observed. $EuO^+(CO)$ may undergo a switching reaction with N_2O to produce the concomitant rise in $EuO^+(N_2O)$. Alternatively, $EuO^+(N_2O)$ may be produced directly in a termolecular reaction of type 21 with CO acting as the third body.

$$EuO^+ + N_2O + CO \rightarrow EuO^+(N_2O) + CO \qquad (21)$$

N_2O addition to YbO^+ appears to poison the catalysis as $YbO^+(N_2O)$ appears not to be reduced by CO; the $YbO^+(N_2O)$ signal declines in response to the decline in the precursor ion instead (see Figure 3).

3.4. Catalytic Cycles and Steady State. For O-atom transport catalysis to be effective, both legs of the catalytic cycle, given by reactions 8 and 9 and shown in Scheme 1, must be rapid. Both of these reactions occur in the reaction region of the flow tube with the 10 MO^+ ions that were observed to produce M^+ by reaction with CO because of the presence of N_2O added upstream to produce MO^+ from M^+. Consequently the catalytic cycle shown in Scheme 1 can be expected to achieve steady state within the reaction region, since the half-lives of the oxidation and reduction reactions ($<10^{-5}$ s) are much shorter than the total reaction time (ca. 5 ms). The steady state was monitored with plots of $[M^+]/[MO^+]$ versus CO flow, since $d[M^+]/dt = d[MO^+]/dt = 0$, and as a consequence, $[M^+]/[MO^+] = k_9[CO]/(k_8[N_2O])$ at steady state. Families of such plots are shown in Figure 4 for $M^+/MO^+ = Fe^+/FeO^+$, Ge^+/GeO^+, Pt^+/PtO^+, and PtO^+/PtO_2^+, each at three different flows of N_2O. It is perhaps surprising at first glance that no effects are seen of the approach to steady state at low CO flows, but this is consistent with the relative magnitude of the half-lives of the oxidation and reduction reactions ($<10^{-5}$ s) and the total reaction time (ca. 5 ms).

The observed linearity in these plots is indicative of the attainment of steady state and provides a measure of k_8/k_9 when the flow of N_2O is known. Table 2 provides a summary of the values of k_8/k_9 determined from the observed linearities in plots of $[M^+]/[MO^+]$ vs CO flow. Knowledge of k_8/k_9 allows the determination of k_9 when k_8 is measured independently in the absence of CO as we have done for the systems investigated here. Table 3 provides average values of k_8/k_9, and values of k_9 determined in this fashion are included in Table 1. In the case of Pt^+/PtO^+ and PtO^+/PtO_2^+ a slight dependence was observed for k_8/k_9 on the N_2O flow (see Table 2). This is attributed to the reduction of the respective higher-order species (PtO_2^+ and $PtO_3^+/PtO_2^+{\cdot}N_2O$) which provide an increasing source for PtO^+ and PtO_2^+ with N_2O flow. The values of k_8/k_9 reported for Pt^+/PtO^+ (0.53) and PtO^+/PtO_2^+ (2.6) are those obtained by extrapolation to zero N_2O flow. Higher oxides were not observed with Ca^+ and Ba^+, and their monoxide clusters were too small to provide a significant source of the monoxide cations. This means that the scatter in the values for k_8/k_9 shown in Table 2 in these two cases is a measure of experimental uncertainty.

Generally speaking, the reduction of N_2O by M^+ that occurs in the reaction region can be sufficiently exothermic to leave

---

[21] Koyanagi, G. K.; Bohme, D. K. *J. Phys. Chem. A* **2001**, *103*, 8964.

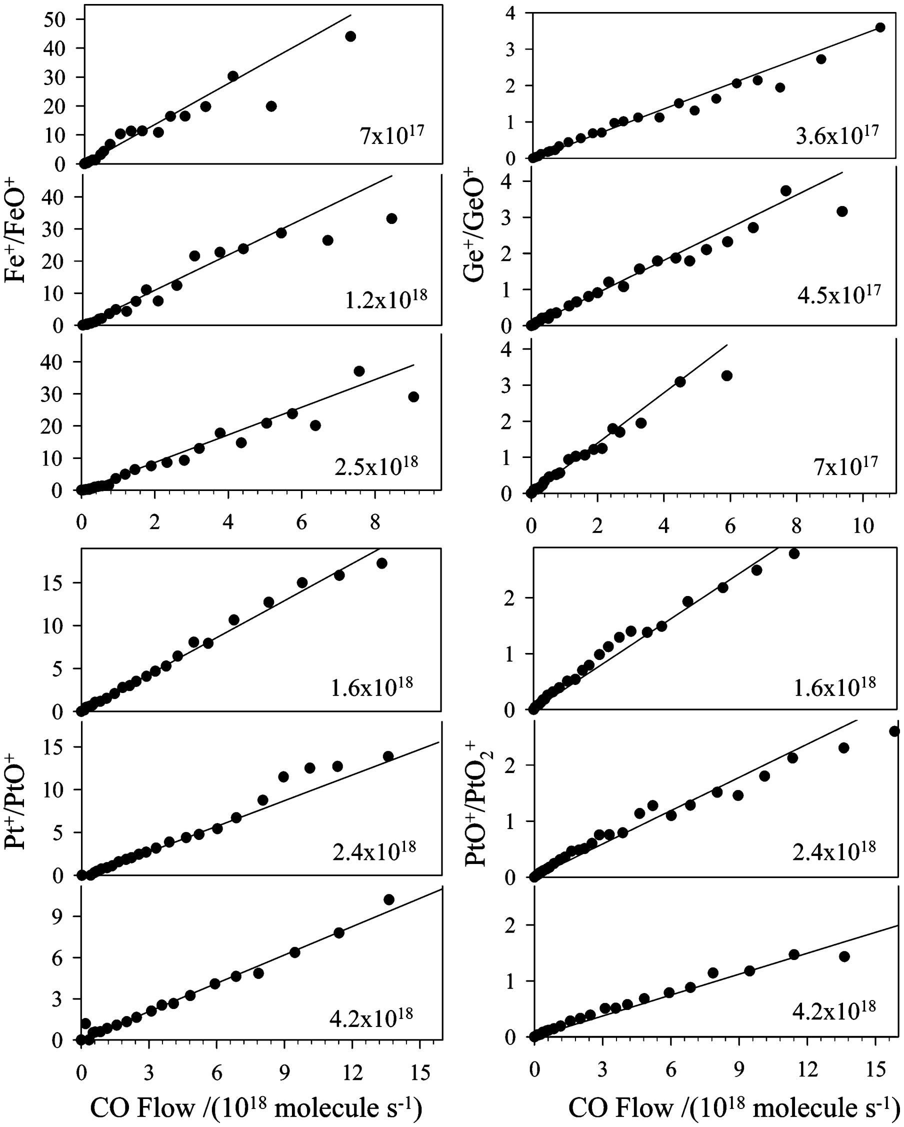

Figure 4. Plots demonstrating the attainment of steady state for the catalytic cycles involving Fe^+ (top left), Ge^+ (top right), Pt^+ (bottom left), and PtO^+ (bottom right) at various flows of N_2O given in the bottom right-hand corner in units of molecules s^{-1}.

MO^+ with some internal excitation. This internal excitation may not be sufficiently quenched by the number of collisions with He buffer gas and N_2O to be thermalized before reacting with CO. Similarly, the M^+ produced in the oxidation of MO^+ by CO may be produced with some internal and kinetic excitation that may not be sufficiently quenched by the number of collisions with He buffer gas and added CO to be thermalized before reacting with N_2O; viz. the catalysis may be proceeding under nonthermalized conditions. However, this appears not to be the case in the experiments reported here at the operating conditions in the reaction region of the flow tube in which He is in large excess. Within the uncertainty of the measurements, the values obtained for k_8/k_9 appear to be independent of the N_2O flow (or nearly so for Pt^+ and PtO^+), and the plots of appear linear over the entire range of CO flow. Generally speaking, this can be expected to be the case in the presence of a buffer gas in sufficiently large excess to ensure thermalization and of course also when k_8 and k_9 are insensitive to internal excitation. Also, the N_2O and CO dependence will be minimal for catalytic couples in which the excitation of ions produced in the individual steps is minimal. For the metal cations investigated here that lie within the thermodynamic window, a low exothermicity in one of the two steps will mean high exothermicity in the other step, since $\Delta H_1 + \Delta H_2 = \mathrm{OA}(N_2O) - \mathrm{OA}(CO)$. In the case of the Fe^+/FeO^+ cycle, the presence of thermalization can be further tested, since both k_8 and k_9 have been measured independently with thermalized ions. The value for $k_9 = 2.4(\pm 40\%) \times 10^{-10}$ cm^3 $molecule^{-1}$ s^{-1} derived here from k_9/k_8 agrees, within experimental error, with the value of $2.05(\pm 30\%) \times 10^{-10}$ cm^3 $molecule^{-1}$ s^{-1} reported earlier in an independent study of the reaction of FeO^+ thermalized upstream of the flow tube with CO added to the reaction region.[3]

The observed reduction of higher oxide cations of Os, Ir, and Pt according to reaction 18 and their formation by oxidation with N_2O as described previously[8] define coupled catalytic cycles as the one shown for Os in Scheme 2 which leads to the reduction of N_2O by CO. The rapid disappearance of the higher oxide cations prevented the evaluation of k_{ox}/k_{red} in these cases. The one exception is the PtO^+/PtO_2^+ cycle for which we were able to determine $k_{ox}/k_{red} = 2.6$.

Also, the observed occurrence of reactions of N_2O adduct ions with CO of type 14a with M = Fe and Pt involving N_2O

Table 2. Summary of Measurements of $k_8/\ k_9$ at Different Flows of N_2O

catalytic ions	N_2O flow (molecules s^{-1})	k_8/k_9
Ca^+/CaO^+	1.3×10^{18}	0.56
Ca^+/CaO^+	2.5×10^{18}	0.79
Fe^+/FeO^+	0.3×10^{18}	0.22
Fe^+/FeO^+	0.7×10^{18}	0.21
Fe^+/FeO^+	1.3×10^{18}	0.20
Fe^+/FeO^+	2.5×10^{18}	0.20
Ge^+/GeO^+	0.9×10^{18}	0.17
Ge^+/GeO^+	1.3×10^{18}	0.17
Ge^+/GeO^+	1.8×10^{18}	0.18
Ba^+/BaO^+	1.5×10^{18}	12.0
Ba^+/BaO^+	2.1×10^{18}	9.1
Pt^+/PtO^+	0.4×10^{18}	0.54
Pt^+/PtO^+	1.7×10^{18}	0.41
Pt^+/PtO^+	2.4×10^{18}	0.41
Pt^+/PtO^+	4.2×10^{18}	0.35
PtO^+/PtO_2^+	0.4×10^{18}	2.6
PtO^+/PtO_2^+	1.7×10^{18}	2.0
PtO^+/PtO_2^+	2.4×10^{18}	1.8
PtO^+/PtO_2^+	4.2×10^{18}	1.5

Table 3. Values for $k_8/\ k_9$ Obtained from the Steady-State Analysis (see Table 2)[a]

catalytic ions	k_8/k_9[b]	E_{ox}[c]	E_{red}[c]	E_{cycle}[d]
Ca^+/CaO^+	0.70	0.17	0.32	0.054
Fe^+/FeO^+	0.21	0.043	0.24	0.010
Ge^+/GeO^+	0.17	0.44	0.28	0.12
Sr^+/SrO^+	0.63	0.080	0.14	0.011
Ba^+/BaO^+	10.6	0.32	0.033	0.011
Os^+/OsO^+	180[e]	0.082	NA	NA
Ir^+/IrO^+	0.85	0.41	0.51	0.21
Pt^+/PtO^+	0.53	0.17	0.34	0.058
Eu^+/EuO^+	NA	0.097	NA	NA
Yb^+/YbO^+	0.06	9.3×10^{-4}	0.018	1.7×10^{-5}
PtO^+/PtO_2^+	2.6	0.82	0.32	0.26

[a] Also included are the reaction efficiencies for the oxidation and reduction steps and the efficiency of the complete catalytic cycle all at 295 K (see text). [b] The uncertainties represent the precision of the measurements. Unless indicated otherwise, the estimated accuracy is ±20%. NA indicates that the required rate coefficients were not available. [c] E_{ox} and E_{red} are equal to the ratio of the reaction-rate coefficient to the collision-rate coefficient, $(k/k_c)_8$ and $(k/k_c)_9$, respectively. [d] The absolute accuracy in the value of E_{cycle} is estimated to be less than 60%. [e] This value should be regarded as an upper limit because of overlap of OsO^+ with unreactive OsN^+.

Scheme 2

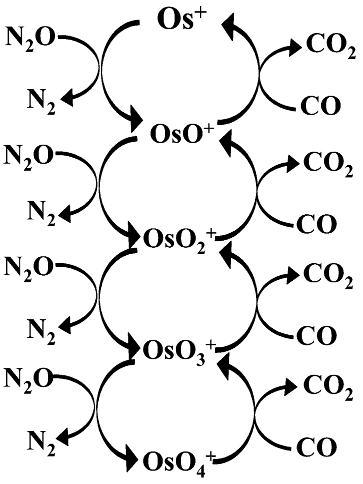

Scheme 3

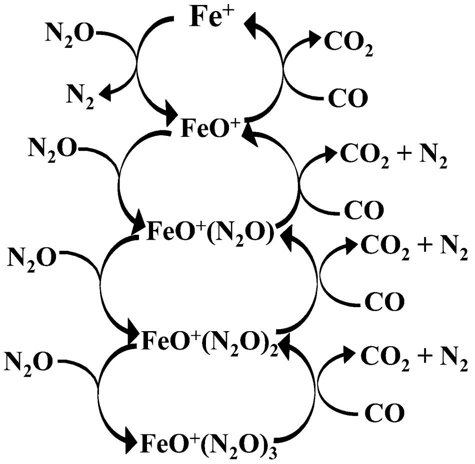

adduct ions and their formation by addition to the metal oxide cation[8] define coupled catalytic cycles as the one shown for Fe in Scheme 3 which also leads to the reduction of N_2O by CO. The rapid disappearance of these adducts again prevented a steady-state analysis.

3.5. Potential Energy Landscape for Catalysis. The potential-energy landscape computed for the reduction of N_2O by CO catalyzed by $Fe^+(^6D)$ according to reactions 1 to 3 is shown in Figure 5. All the intermediates and transition state structures on the catalyzed pathway are in the sextet electronic state. The uncatalyzed reduction shown in the top profile proceeds in one step via a high activation barrier of 47.2 kcal mol^{-1} and is strongly exothermic, by 86.7 kcal mol^{-1} according to the calculations and by 87 kcal mol^{-1} according to published enthalpies of formation.[6] The structure of the transition state corresponds to a direct attack of oxygen atom of N_2O on the carbon atom of CO. The N−O bond is being broken, and the C−O bond is being formed. The activation barrier for the uncatalyzed reduction of N_2O by CO, apparently due to the cleavage of the N−O bond, is lowered by more than a factor

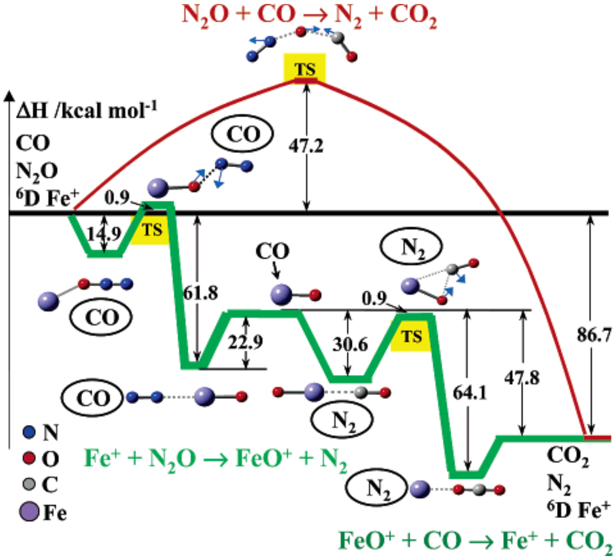

Figure 5. Energy landscape for the reduction of N_2O by CO in the absence and presence of Fe^+ (^6D) computed using DFT with hybrid B3LYP exchange-correlation functional and a triply split 6-311+G(d) basis set with one set of diffuse and polarization functions. The red profile corresponds to the neutral reaction of N_2O with CO. The green profiles correspond to the linked catalytic ion−molecule reactions of Fe^+ with N_2O and of FeO^+ with CO. The bold black line corresponds to the dissociation limit to Fe^+, N_2O, and CO. Spectator molecules are in indicated in ovals. Transition state structures are labeled with TS; transition state vectors are sketched.

of 50 to a mere 0.9 kcal mol^{-1} that arises in the first step of the much faster ionic path. The reaction coordinates of both ionic steps in this path are described by double-minimum potential-energy profiles. The first step involves O-atom transfer from N_2O to Fe^+ with the formation of FeO^+ and N_2. The activation barrier is 0.9 kcal mol^{-1} above the dissociation limit. This is somewhat lower than the barrier of 4.2 kcal mol^{-1} that we predicted recently using the B3LYP/sdd/6-311+G(d) method with the relativistic ECP and a double-ζ basis set for iron.[8] The higher value obtained might be attributable to the limitations of the ECP and basis set that was used. The second step in the catalyzed reduction of N_2O by CO involves O-atom transfer from FeO^+ to CO with the formation of Fe^+ and CO_2 and proceeds without a barrier. The energy of the transition state in the second step lies 0.9 kcal mol^{-1} below the dissociation limit to FeO^+ and CO.

The catalysis in the reaction region of the flow tube proceeds in a helium bath at a pressure of 0.35 Torr so that any excess energy that appears in FeO^+ produced in the first step of the catalysis is relaxed by many collisions with He atoms before FeO^+ collides with CO and can complete the catalysis.

3.6. Efficiency of Catalysis. The so-called "turnover number", N, defined as the number of molecules converted by one catalytic ion, is often used as a numerical measure of the efficiency of catalysis. Numerically it is given by the expression $N = \phi/(1 - \phi)$ where ϕ is the fraction of the catalytic channel in the reaction cycle ($\phi = \phi_1\phi_2$ if each leg of the cycle is fractionally depleted by competing channels). When the only channel is the catalytic channel, viz. in the absence of any competing channels, as is the case in Scheme 1, and for all but two of the 10 atomic catalytic redox couples observed in this study, ϕ is > 0.99 and N is > 99. The "intrinsic" turnover number defined in this way therefore is not very useful for distinguishing the relative merits of these catalytic cations. Os^+ is an exception because of OsN^+ formation and Eu^+ because EuO^+ clusters with CO; both competing channels act to reduce the turnover number. To be sure, in a real chemical system, the intrinsic turnover number would be modified (reduced) by the presence of gases that react with M^+ or MO^+ in another fashion and so compete with the catalytic cycle.

We propose here, for the first time, a measure of the intrinsic efficiency, E_{cycle}, for individual catalytic cycles in order to allow a quantitative measure of the relative intrinsic merits of catalytic cations *in the absence of competing reaction channels*. We explicitly take into account the reaction efficiency of each of the two legs of such cycles and so define E_{cycle} as shown in eq 22

$$\text{Efficiency, } E_{\text{cycle}} = E_{\text{ox}} \times E_{\text{red}} = (k/k_c)_8 \times (k/k_c)_9 \quad (22)$$

in terms of the product of the reaction efficiency, $E = k/k_c$, for each of the two component reactions of the catalytic cycle, the oxidation reaction 8 and the reduction reaction 9 in our case. According to this definition the efficiency E_{cycle} has a maximum value of 1 (or 100%). Perhaps we should emphasize that E_{cycle} defined in this way, on a per cycle basis, does not replace the turnover number as a measure of the overall efficiency of catalysis which becomes useful in the presence of competing reaction channels. However, the definition of E_{cycle} also could be extended to take into account competing reaction channels by multiplying E_{ox} by ϕ_{ox} and E_{red} by ϕ_{red}, but this approach still should be restricted to a measure of E_{cycle} for individual catalytic cycles.

If a temperature is to be ascribed to E_{cycle}, then it is necessary that the measured reaction-rate coefficients correspond to thermalized conditions at a known temperature. Otherwise the measured efficiency becomes an instrumental artifact. In the absence of thermalization the instrumental efficiency will be influenced by the partitioning of the excess energy of the oxidation and reduction reactions and so perhaps on the position of $OA(M^+)$ in the thermodynamic window for O-atom transport. Of course any kinetic barriers that influence the magnitude of the reaction-rate coefficients for oxidation and reduction will influence the magnitude of E_{cycle}. Since N_2O and CO_2 and N_2 and CO are isoelectronic with the same spin configuration, any spin constraints in one step would be a constraint in the other step in the catalysis and lead to lower values for E_{cycle}, although details of the crossings of the spin surfaces may differ.

The experimental rate coefficients used in the calculation of the efficiencies, E_{cycle}, for the catalytic cycles reported here were as follows. The values for k_8 were taken from measurements reported previously in which the atomic ions were generated in the same ICP source as used here and in which N_2O was added into the reaction region downstream of the flow tube (in the absence of CO).[8] Even though the catalytic cations produced within the ICP have substantial excited-state populations at their point of origin, there were no indications of excited-state effects in these measurements of k_8.[8] The values for k_9 used in the calculation of E_{cycle} were derived from the steady-state analyses presented above which provide a measure of k_8/k_9 as already indicated.

Efficiencies computed according to eq 22 for the catalytic atomic cations identified in our study are included in Table 3 where they are seen to range from 1.7×10^{-5} (for Yb^+/YbO^+) to 0.21 (for Ir^+/IrO^+). They indicate the following order of efficiency: Ir^+/IrO^+ (0.21) > Ge^+/GeO^+ (0.12) > Pt^+/PtO^+ (0.058) = Ca^+/CaO^+ (0.054) > Sr^+/SrO^+ (0.011) = Ba^+/BaO^+ (0.011) = Fe^+/FeO^+ (0.010) > Yb^+/YbO^+ (1.7×10^{-5}). The positions of the 10 M^+ cations identified as catalysts on the periodic table are indicated in Figure 6. Also included in Table 3 is the efficiency (0.26) of the one catalytic diatomic cation (PtO^+) identified in the study. This efficiency is the highest among all the cations investigated.

The main-group metal cation Ge^+ (p^1) has $OA(Ge^+) = 81.8$ kcal mol^{-1} which is about in the middle of the thermodynamic window, halfway between 40 and 127 kcal mol^{-1}. So both legs of the catalytic cycle are equally exothermic; they have about equal efficiencies: $E_{\text{ox}} = 0.44$ and $E_{\text{red}} = 0.28$. The overall efficiency for the cycle is relatively high (12%). We suspect that the known value $OA(Ir^+) = 59$ kcal mol^{-1} should actually be 15 kcal mol^{-1} higher based on our observation of O-atom transfer of NO_2 to Ir^+ (d^7s^1).[5] So $OA(Ir^+)$ may also lie in the middle of the thermodynamic window for catalysis. Again, both legs have relatively high efficiencies, $E_{\text{ox}} = 0.41$ and $E_{\text{red}} = 0.51$ and $E_{\text{cycle}} = 21\%$. Intermediate values are associated with E_{cycle} for Pt^+ (5.8%) and Ca^+ (5.4%) for which OA = 77 kcal mol^{-1}. Fe^+(d^6s^1), Sr^+ (s^1), and Ba^+ (s^1) all have values for E_{cycle} of about 1% at room temperature. Values for OA are 80.0, 71.4, and 92.8 kcal mol^{-1}. Fe^+ and Sr^+ exhibit inefficient oxidation (Fe^+ has actually been shown to have a small kinetic barrier).[8] In contrast, the cycle with Ba^+ has an inefficient reduction step.

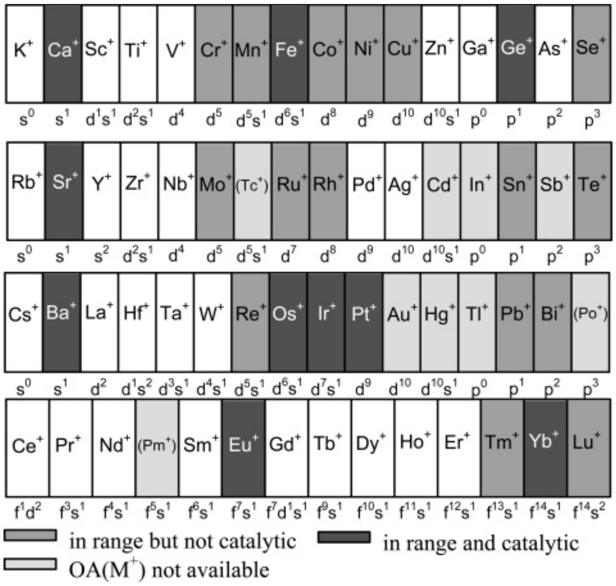

Figure 6. Periodic table showing atomic cations that lie in the thermodynamic window for O-atom transport catalysis of the reduction of N_2O by CO and those that have been demonstrated to be catalytic.

It is interesting to note that there is a systematic decrease in E_{red} for the rare-earth cations down the periodic table from 0.32, 0.14, and 0.033 for CaO^+, SrO^+, and BaO^+, respectively, perhaps because of increased charge delocalization with the increasing size of the metal cation. The very low cyclic efficiency for Yb^+ is due to the low oxidation efficiency that has been attributed to an electron-promotion energy effect.[19]

Our failure to measure a cyclic efficiency for the 16 other atomic cations that lie within, or perhaps just outside, the thermodynamic window for catalysis can be attributed primarily due to a low oxidation efficiency. The nonreactions involving Cr^+/CrO^+, Mn^+/MnO^+, Co^+/CoO^+, Ni^+/NiO^+, Mo^+/MoO^+, and Ru^+/RuO^+ have previously been ascribed to spin constraints.[8] A low oxidation efficiency of course often prevented the measurement of the efficiency of reduction.

Conclusions

The catalytic action of atomic cations in the reduction of N_2O by CO has been identified as O-atom transport constrained thermodynamically in terms of a "thermodynamic window of opportunity" some 87 kcal mol^{-1} wide. With this window as a guide, an expanded search for atomic-cation catalysts has identified 6 new catalysts in addition to 4 that have been reported previously. The total of 10 is much less than the 26 of 59 that fall within the window. The remaining 16 potential catalysts are eliminated by kinetic constraints that arise from various causes, although 2 of these 16 potential catalysts may well lie outside this window.

Steady state was achieved in the reaction region of the ICP/SIFT tandem mass spectrometer that allowed the measurement of an efficiency for cyclic catalysis, E_{cycle}, defined here for the first time for catalytic cations *in the absence of competing reaction channels*. E_{cycle} is defined in a manner that allows it to respond to varying efficiencies for the two legs of the catalytic cycle, E_{ox} and E_{red}, and so discriminate between the performance of catalytic cycles in which competing channels are absent. This is not possible with the traditional use of the "turnover number" which would be infinite for all these cycles. Efficiencies for cyclic catalysis, E_{cycle}, are reported for eight atomic cations and one diatomic cation.

The potential-energy landscape computed for the reduction of N_2O by CO catalyzed by $Fe^+(^6D)$ provides a striking illustration of the operation and power of an ionic catalyst.

Acknowledgment. Continued financial support from the Natural Sciences and Engineering Research Council of Canada is greatly appreciated. Also, we acknowledge support from the National Research Council, the Natural Science and Engineering Research Council and MDS SCIEX in the form of a Research Partnership grant. As holder of a Canada Research Chair in Physical Chemistry, Diethard K. Bohme thanks the contributions of the Canada Research Chair Program to this research.

Supporting Information Available: Electronic energies and enthalpies at 0 K and Cartesians coordinates predicted for the reactions $N_2O + CO \rightarrow N_2 + CO_2$; $Fe^+ + N_2O \rightarrow FeO^+ + N_2$; and $FeO^+ + CO \rightarrow Fe^+ + CO_2$ (for Figure 5) with the B3LYP/6-311+G* method. This material is available free of charge via the Internet at http://pubs.acs.org.

JA044950M